Weierstraß-Institut
für Angewandte Analysis und Stochastik
Leibniz-Institut im Forschungsverbund Berlin e. V.

Preprint ISSN 0946 – 8633

Spatial “rocking” for improving the spatial quality of the beam of broad area semiconductor lasers

Mindaugas Radziunas[1], Kestutis Staliunas[2,3]

submitted: April 25, 2012

[1] Weierstrass Institute
Mohrenstr. 39
10117 Berlin, Germany
E-Mail: Mindaugas.Radziunas@wias-berlin.de

[2] Departament de Física i Enginyeria Nuclear
Universitat Politècnica de Catalunya
Colom 11
08222 Terrassa, Barcelona, Spain

[3] Institució Catalana de Reserca i Estudis Avançats (ICREA)
Pg. Lluis Companys, 23
08010 Barcelona, Spain
E-Mail: kestutis.staliunas@icrea.es

No. 1703
Berlin 2012

2010 *Mathematics Subject Classification.* 78A60, 35B36, 37M05, 78A45.

2008 *Physics and Astronomy Classification Scheme.* 42.55.Px, 42.65.Pc, 42.60.Jf.

Key words and phrases. Broad area semiconductor laser, traveling wave model, off-axis optical injection, stabilization, focusing, rocking .

The work of M. Radziunas was supported by DFG Research Center MATHEON “Mathematics for key technologies: Modelling, simulation and optimization of the real world processes”.

Edited by
Weierstraß-Institut für Angewandte Analysis und Stochastik (WIAS)
Leibniz-Institut im Forschungsverbund Berlin e. V.
Mohrenstraße 39
10117 Berlin
Germany

Fax: +49 30 2044975
E-Mail: preprint@wias-berlin.de
World Wide Web: http://www.wias-berlin.de/

Abstract

The spatial "rocking" is a dynamical effect converting a phase-invariant oscillatory system into a phase-bistable one, where the averaged phase of the system locks to one of two values differing by π. In this paper we consider theoretically the spatial rocking of irregularly operating edge emitting broad area semiconductor laser. The stabilization of the laser is realized by the injection of an optical field formed by two, coherently interfering at some angle, beams. We demonstrate that this stabilization is preserved if one or both injected beams are weakly focused, and analyze a corresponding focusing of the emitted field.

Broad area semiconductor laser, traveling wave model, off-axis optical injection, stabilization, focusing, rocking

1 Introduction

The effect of "rocking" has been proposed as a general phenomenon in physics of dynamical systems, which converts the phase-invariant oscillatory system into a phase-bistable one where the average phase of the system locks to one of two values differing by π [1, 2]. Many nonlinear systems in nature and in technics display self-sustained oscillations with a particular amplitude and invariant phase. If such system is subjected to a nearly-resonant additive signal, then the phase invariance of oscillations can be broken, and the frequency and phase of the system can lock to that of the external signal. If the complex amplitude of external injection becomes periodic in time, e.g. follows the harmonic oscillation law $\sin(\Omega t)$, then a pair of stable states with similar amplitudes but opposite phases can be obtained [1]. For the systems of a large number of space degrees of freedom, e.g. for the resonator with a large Fresnel number, the "rocking" results in excitation of spatial patterns such as rolls, phase domain walls and phase solitons [3]. Such patterns are typical for the phase-bistable spatially extended systems [4, 5, 6, 7, 8].

Later, the *spatial* "rocking" was proposed, where the complex amplitude of injection is a π-alternating periodic function *in space* on a relatively small space scale [9, 10]. The spatial rocking, similarly to the temporal rocking, results in a phase-bistable dynamics of a "small" system with a relatively small number of the space degrees of freedom, and in phase-bistable patterns in a spatially extended system. The spatial rocking in infinitely spatially extended systems has been predicted for a general case of dynamical systems, on basis of the model of the periodically in space driven complex Ginzburg-Landau equation [9]. In addition, a "simplified" spatial rocking is possible in systems of a limited spatial extend, i.e. in the systems supporting several transverse modes. The rocking in such systems of finite number of spatial degrees of freedom has been proposed theoretically [10] and confirmed experimentally [11].

Recently, the phase-bistable dynamics and the most simple transverse patterns were demonstrated by us theoretically in the system with neither "large", nor "small" aspect ratio [12]. All these effects were shown in simulations of the 2+1 dimensional traveling wave model describing the dynamics of a broad area (BA) edge-emitting semiconductor laser, which is a widespread and practically relevant system [13, 14, 15, 16]. The spatial rocking in this case is realized by a periodic in space injection formed by two, coherently interfering at some angle, beams (see Fig. 1).

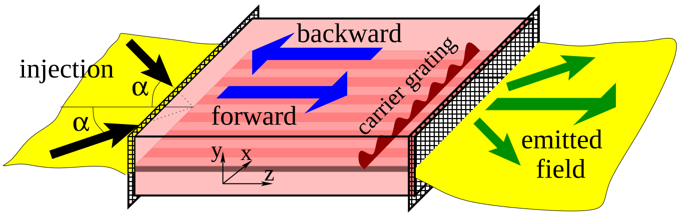

Figure 1: Schematic representation of the simulated optically injected broad area laser.

In the present paper we continue our study of the field stabilization in BA lasers depending on properties of the applied optical injection. Namely, we analyze an impact of the focusing of the injected beams to the stabilization of the laser emission.

2 Mathematical model

Like in our preceeding paper[12] we consider the following TW model [13, 14, 15] for BA lasers:

$$\begin{aligned}
\frac{\partial}{\partial t}E^{\pm}(t,x,z) &= \tfrac{c}{n_g}\left(\tfrac{-i}{2k_0\bar{n}}\partial_{xx} \pm \partial_z - i\beta - \tfrac{\bar{g}}{2}\right)E^{\pm} + \tfrac{c}{n_g}\tfrac{\bar{g}}{2}p^{\pm}, \\
\frac{\partial}{\partial t}p^{\pm}(t,x,z) &= \tfrac{k_0 c}{2\lambda_0}\bar{\Gamma}\left(E^{\pm}-p^{\pm}\right) - \tfrac{ik_0 c}{\lambda_0}\bar{\lambda}_0 p^{\pm}, \\
\frac{\partial}{\partial t}N(t,x,z) &= d_N\partial_{xx}N + \tfrac{J(x,z)}{qd} - \left(AN+BN^2+CN^3\right) \\
&\quad -\tfrac{c}{n_g}\Re e\sum_{\nu=\pm}E^{\nu *}\left(\left(g\left(N,E^{\pm}\right)-\bar{g}\right)E^{\nu}+\bar{g}p^{\nu}\right).
\end{aligned} \tag{1}$$

Here, t denotes time, z – the longitudinal coordinate, along the propagation direction, x – the transverse coordinate. $E^{\pm}(t,x,z)$ are the complex slowly varying amplitudes of the forward and backward traveling optical fields, so that $|E|^2 = |E^+|^2 + |E^-|^2$ denotes the local photon density. At the laser facets the optical fields satisfy the boundary conditions

$$E^{+}(t,x,0) = r_0 E^{-}(t,x,0) + a(t,x), \quad E^{-}(t,x,l) = r_l E^{+}(t,x,l), \tag{2}$$

where $a(t,x)$ denotes the optical field injected into the laser through the left facet. Functions $p^{\pm}(t,x,z)$ are the complex slowly varying amplitudes of induced polarization used to model the Lorentzian wavelength dependence of the optical gain. close to its maximum. $N(t,x,z)$ is the real-valued distribution of excess carrier density. The injection current density J is given by

$$J(x,z) = \begin{cases} I/lw, & \text{if} \quad (x,z)\in S = \left\{\left(-\frac{w}{2},\frac{w}{2}\right)\times(0,l)\right\} \\ 0, & \text{otherwise} \end{cases},$$

were S and I denote the laser area (l: length, w: width) and the injection current, respectively. The complex propagation factor β, the peak gain function g, and the refractive index change function δ_n are given by

$$\beta = \delta_n(N) + i\frac{g(N, E^{\pm}) - \gamma}{2}, \quad g(N, E^{\pm}) = \frac{g' \ln(N/N_{tr})}{1 + \epsilon|E|^2}, \quad \delta_n(N) = -k_0\sqrt{n'N}.$$

$k_0 = 2\pi/\lambda_0$, c, q and h are the central wavenumber, the speed of light in vacuum, the electron charge, and the Planck constant, respectively. The values and the brief explanation of all parameters are given in Table 1 and Refs. [15, 16]. To resolve long transients and to perform a parameter continuation of the system in a reasonable time we have used high performance parallel distributed computing algorithms [15]. Comparable computations on a single PC system take nearly 100 times longer.

Table 1: Parameters used in simulations.

λ_0	central wavelength	973 nm	N_{tr}	transparency carrier density	1.3·10^{18} cm^{-3}
$\bar{n}$	reference refractive index	3.2262	A	recombination parameter	0.295·10^9 s^{-1}
n_g	group refractive index	3.66	B	recombination parameter	1.8·10^{-10} cm^3/s
g'	differential gain	23.4 cm^{-1}	C	recombination parameter	3.28·10^{-30} cm^6/s
n'	differential index	1.25·$10^{-25}$$cm^3$	$\bar{\lambda}_0$	gain peak detuning	0 nm
γ	internal absorption	1.5 cm^{-1}	$\bar{\Gamma}$	Lorentzian width at half max.	80 nm
I	injection current	3 A	$\bar{g}$	Lorentzian gain amplitude	130 cm^{-1}
d_N	carrier diffusion coefficient	19.672 cm^2/s	r_0	left facet ampl. reflectivity	-0.3
l	length of the laser	1.5 mm	r_l	right facet ampl. reflectivity	0.3
w	width of the laser	0.2 mm	α	angle of the optical injection	0.05 rad.
d	depth of the active region	16 nm	ω_{in}	optical frequency of injection	0
ϵ	nonlinear gain compression	5·10^{-18} cm^3	$\mu^{\pm}$	focusing factors	0, 0.5·10^{-5}

In contrast to our previous paper[12] were $a(t, x)$ was determined by the interference of two perfect plane waves of opposite angles α and $-\alpha$ with respect to the optical axis of the laser, in the present study we assume that one or both branches of the injected field are focused. I.e., we consider the optical injection of the following form:

$$\begin{aligned} a\,(t,x) &= a_0 e^{i\omega_{in}t}\tfrac{e^{i\alpha k_0 x}e^{i\mu^+(k_0x)^2} - e^{-i\alpha k_0 x}e^{i\mu^-(k_0x)^2}}{2i} \\ &= a_0 e^{i\omega_{in}t} e^{i\frac{\mu^+ + \mu^-}{2}(k_0x)^2} \sin\left(\alpha k_0 x + \tfrac{\mu^+ - \mu^-}{2}(k_0x)^2\right). \end{aligned} \tag{3}$$

Parameter ω_{in} is the optical frequency of the injection, relative to the reference frequency $\omega_0 = 2\pi c/\lambda_0$, μ^+ and μ^- represent the focal radii of both focused plane waves, and a_0 is the optical field amplitude determining the power of the optical injection

$$P_{inj} = |a_0|^2 \int_{-w/2}^{w/2} \sin^2\left(\alpha k_0 x + \frac{\mu^+ - \mu^-}{2}(k_0x)^2\right) dx \times \frac{cd}{n_g}\frac{hc}{\lambda_0}.$$

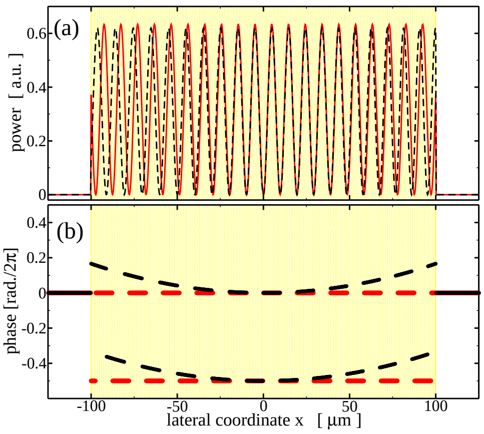

Figure 2: (a): intensity and (b): phase of the optical injection $a(x,0)$. Red: without focusing ($\mu^{\pm} = 0$). Black: with focusing ($\mu^{+} = 0.5 \cdot 10^{-5}$, $\mu^{-} = 0$). Shading: the lateral interval where the BA laser is biased.

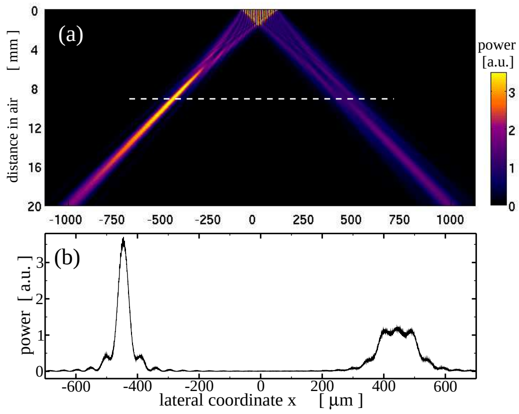

Figure 3: (a): propagation of the focused beam ($\mu^{+} = 0.5 \cdot 10^{-5}$, $\mu^{-} = 0$) in the air, and (b): its intensity distribution at a fixed distance from the source [indicated by the horizontal white dashed line in panel (a)].

Two typical considered optical injection functions $a(x,0)$ are represented in Fig. 2. When the focusing is absent (red lines and dashes), this function is strictly harmonic in x with the peacewise constant periodically alternating phases 0 and $-\pi$. Once a single plane waves is focused (red lines and dashes), the alternating phases are following two parabolas shifted by π with respect to each other. Note also, that the intensity of the input field with a single focused beam is no more strictly periodic: see, e.g., a decreasing oscillation periodicity of the black curve in Fig. 2(a).

The smaller is the focusing factor μ^{-} or μ^{+}, the bigger is the corresponding focal radius. To determine it, we solve numerically the linear Schrödinger equation

$$\partial_z A = \frac{-i}{2k_0}\partial_{xx} A, \quad A(0,x) = A_0(x), \tag{4}$$

governing the propagation of the optical field A in the air, and look for a localization of the field intensity within the beam propagating with the corresponding angle w.r.t. the optical axis of the laser. An initial function $A_0(x)$ in Eq. (4) is determined either by the injected field function $a(t_0,x)$, or by the emitted field $\sqrt{1-|r_l|^2}E^{+}(t_0,x,l)$. Fig. 3 represents the propagation of the injected weakly focused field in the air. Panel (a) of this figure shows the field intensity at different distances from the source. We can clearly recognize the left (focused) and the right (non-focused) propagating off-axis beams. While the intensity of the non-focused beam spreads and decays with an increasing distance from the source, the intensity of the focused beam first reaches its maximum vale at, approximately, 9 mm from the source and only afterwards starts to decay: see also panel (b), where the field intensity distribution close to this focal distance is shown.

3 Stabilization of BA lasers

For the considered injection current I the BA laser is pumped well above the threshold and, in the absence of an optical injection, results in the multi-mode emission, characterized by a random beat of many longitudinal and transverse modes: see column (a) of Fig. 4. In this case, peaks of the optical field intensity [panel (a1)] as well as certain field phases [panel (a2)] can be expected at any lateral position within the BA laser. Rapidly moving and changing field peaks have only a small impact on the carrier density distribution, which remains rather smooth and nearly uniform within the whole BA laser [panel (a3)]. The irregularly oscillating time trace of the emitted field intensity [panel (a4)], the broadened optical spectrum [panel (a5)], the broad time-averaged far field [green line in panel (a6)], the irregular time-averaged near-field phase distribution [green dots in panel (a7)], as well as the irregular instant near-field profile [black curve in panel (a8)] are typical features of an unstable multi-mode operation.

In our previous work [12] we have demonstrated how a properly chosen optical injection (3) with $\mu^{\pm} = 0$ is stabilizing the operation of BA lasers at one of several related stable attractors (spatially-rocked states). Column (b) of Fig. 4 represents one of these stable regimes. A laterally-periodic optical injection with a significant intensity is responsible for the formation of the corresponding lateral grating of the carrier densities [panel (b3)], which itself supports a corresponding lateral optical mode characterized by a parallel-striped structure of its intensity distribution [panel (b1)] with the stripe separation $\lambda_0/2\alpha$ and a typical alternation between more and less intensive stripes [see panel (b8) and the right side of panel (b1)]. The phases of this optical mode [panel (b2) and the black dots in panel (b7)] oscillate in space around some fixed value. The intensity [panels (b4)] of the stabilized laser emission [panels (b4,5)] is ≈ 1.6W, i.e., it is significantly higher then the mean output of the non-injected laser. The optical injection angles $-\alpha$ and α are represented by the outer "ears" in the far field of the emitted light [black curve in panel b6]. These angles determine also the $\lambda_0/2\alpha$-periodicity of the small spatial scale modulation of the optical fields: see, e.g., black dots and curves in the near field pictures (b7,8). Red curves and dots in rows (6-8) show the far and near fields after their averaging over the small space scale. As a consequence of this averaging, the far field looses the outer angular components, the near field intensity becomes relatively homogeneous, and its phase is nearly constant within the central part of the simulated laser device. The central peak of the far field [panel (b6)] represents also an operation of the non-injected laser and its nonlinear interaction with two injected angular beams. We note here, that too strong optical injection will lead to its full dominance over the laser generation. The BA laser in this case will work as an amplifier, and the emitted field will have only two angular components (far field peaks at the angles $-\alpha$ and α).

A similar stabilization of the BA laser can be also achieved if one (column (c) of Fig. 4) or both (column (d) of the same figure) injected off-axis beams are focused. An impact of this focusing is represented by the loss of a nearly perfect parallel structure of the carrier density distribution [see panels (c3) and, especially, (d3)]. We note also a stronger alternation of the near field intensity peaks in panel (d8) and a related enhancement of the central far field peak in panel (d6).

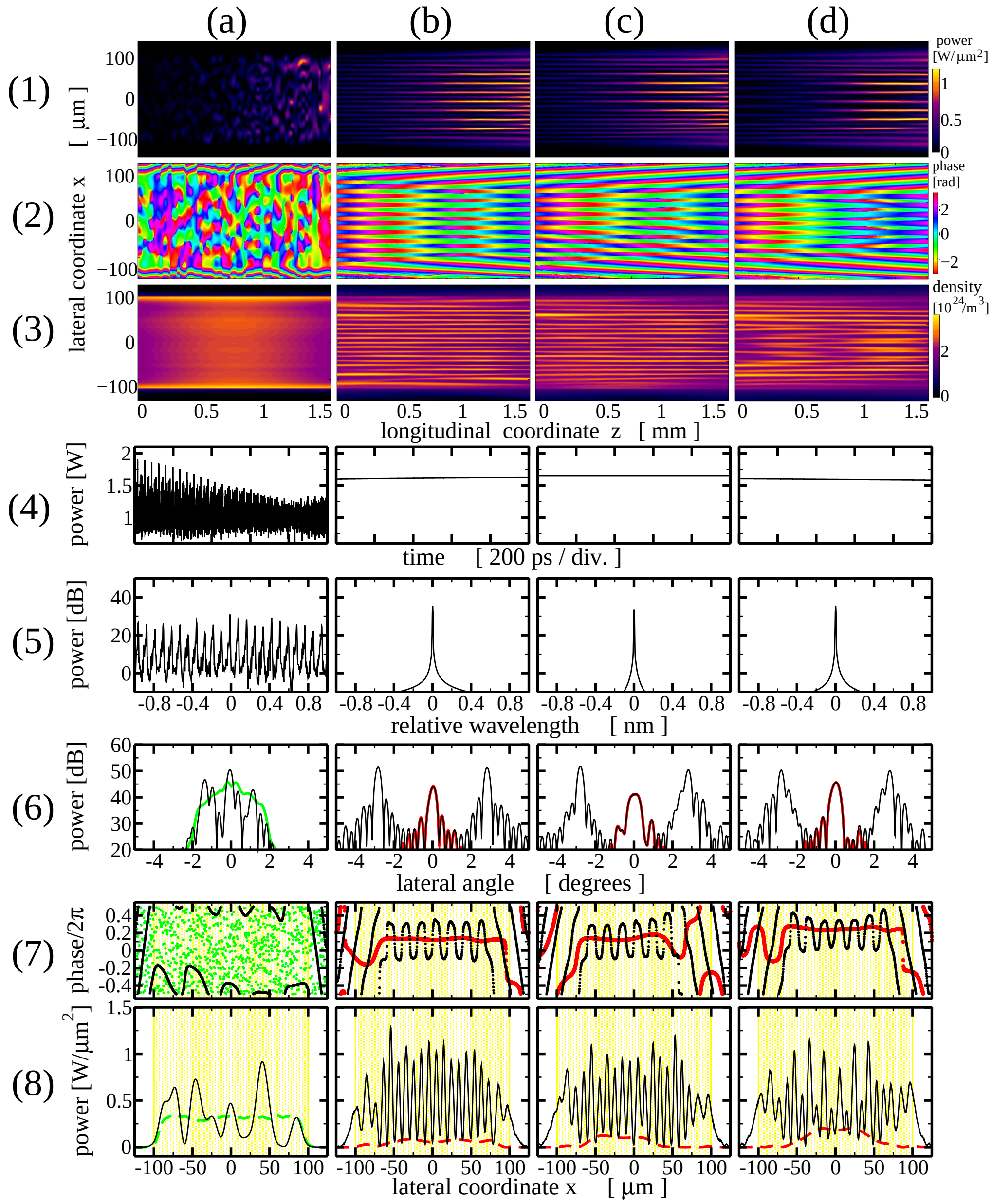

Figure 4: Operation regimes of the BA laser without ($P_{inj} = 0$) and with an optical injection ($\omega_{in} = 0$ and $P_{inj} = 0.2$W). Columns: no injection (a), an injection without focusing [$\mu^{\pm} = 0$] (b), an injection with a single focused beam [$\mu^{+} = 0.5 \cdot 10^{-5}$, $\mu^{-} = 0$] (c), and an injection with both focused beams [$\mu^{\pm} = 0.5 \cdot 10^{-5}$] (d). Rows: spatial distributions of the forward field intensity $|E^{+}(t, x, z)|^2$ (1), its phase (2), and the local carrier density (3) at a fixed moment t. Time traces of the emitted field intensity (4), corresponding optical spectra (5), far fields (6), phases (7) and intensities (8) of the near fields. Green and red curves and symbols in columns (a) and (b-d) indicate time- and small spatial scale averaged quantities, respectively. Black curves and symbols in the same panels show the same quantities for the fixed time moment t. Shading in rows (7,8): the lateral interval where the BA laser is biased.

4 Focusing of the emitted beam

Next, we analyze a propagation of the emitted optical fields in the air, given by the solution of the linear Schrödinger equation (4). Like in previous Section, we consider the BA laser with three different optical injections having the same intensity and optical frequency, but different focusing factors μ^+ and μ^-. The results of this study are summarized in three columns of Fig. 5.

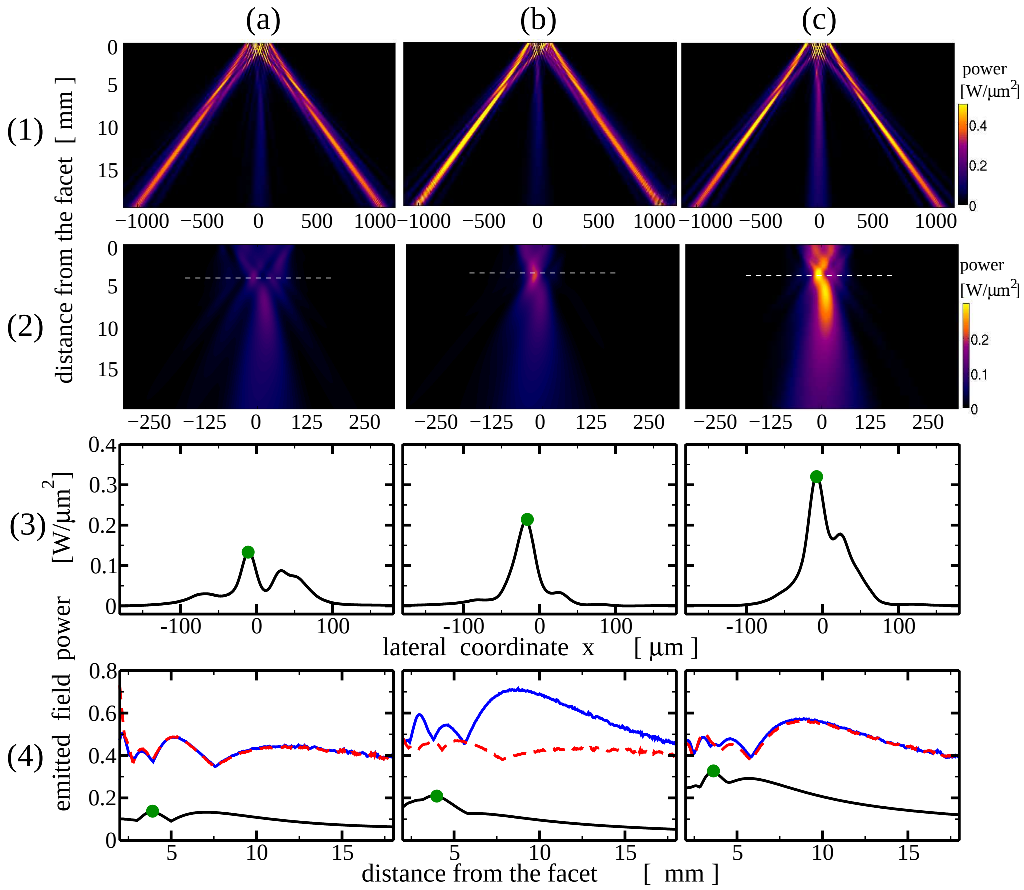

Figure 5: Spreading of the field emitted by the optically injected laser ($\omega_{in} = 0$, $P_{inj} = 0.2$W) in the air. Columns: an injection without focusing [$\mu^{\pm} = 0$] (a), an injection with a single focused beam [$\mu^+ = 0.5 \cdot 10^{-5}$, $\mu^- = 0$] (b), and an injection with both focused beams [$\mu^{\pm} = 0.5 \cdot 10^{-5}$] (c). Rows: spreading of the emitted field (1), of the small-scale-averaged emitted field (2), its intensity distribution at the fixed distance from the facet (3), and a dependence of the maximal intensities of the small-scale-averaged field (black), left- (blue) and right- (red dashed) of-axis beams within the non-averaged field on the distance from the facet (4). Horizontal white dashed lines in row (2) indicate coordinates used to plot the figures of row (3). Green bullets in rows (3,4) indicate absolute maxima of the small-scale-averaged beams.

In the top row panels the intensities of the emitted fields at different distances from the laser facet are shown. The side-propagating beams are implied by the transmission and amplification of the injected off-axis plane waves. A focusing of the original injected beams (if present) implies a spatial localization of the field intensity on the corresponding off-axis branch of the emitted field. The distance of these intensity peaks form the facet is approximately the same as the focal distance of the injected beams [see Fig. 3(a)]. We note also, that the largest intensity of the emitted off-axis beam is achieved in the asymmetric focusing case [blue line in panel (4b)].

In the second row panels the propagation of the small-scale-averaged beams is presented. As it was mentioned in previous Section, this averaging helps us to separate the central part of the emitted field (see first row panels) from the field components propagating at the injection angles $-\alpha$ and $+\alpha$. The most intensive averaged field was observed in the laser with both focused injected beams [panel (2c)]. The lateral field intensity distributions at the selected (focal) distances from the facet show a much better field localization in the focused injection cases [panels (3b,c)]. We note, however, that a weak localization of the averaged field intensity with an increasing distance from the facet (peaks of the black curves in the 4-th row panels) can be seen in all three considered cases. Since the distance between these intensity peaks and the laser facet is similar, we conclude that it has no correlation with the focal distance of the injected beams, and that the BA laser itself performs some small lensing of the optical field.

5 Parameter study

To find the optical injection intensities for which the spatial rocking is efficient we have performed a following parameter study. We have integrated numerically the model equations over 1 ms consequently performing an intermediate estimate of the simulated regime and a fine step-like tuning of P_{inj}. This procedure allows to stay close to the same attractor in the phase space, to follow deformations of this attractor with the change of parameters, to detect its bifurcations and eventual transitions to another attractor. The results of such one-parameter continuation for the BA laser with three different types of the injected field are summarized in Fig. 6.

The unstable irregular multi-mode dynamical regime indicated as "regime A" in top panels of Fig. 6 is observed for all small injection intensities P_{inj}. In the case of a sufficiently large injection (e.g., just before the transition to the regime "B"), we can also have some partial coherence of different modes implying the formation of still incomplete phase patterns [12]. In general, such multi-mode regimes are typical for BA lasers without optical injection (see, e.g., the simulated state presented in column (a) of Fig. 4). The spatial rocking discussed in previous Sections is a typical representative of the dynamical regime indicated as "regime B" in top panels of Fig. 6. It is, first of all, a continuous wave state possessing a single sharp line in the optical spectra [first row panels] and having no modulation of the emitted field intensity [5-th row panels]. In addition, the rocked state should have a flat nearly constant phase of the small-scale-averaged emitted field [3-rd row panels], and a non-vanishing zero-angle contribution in its far field [2-nd row panels], which monotonously decays with an increase of the optical injection intensity. Otherwise, for too large P_{inj} ("regime C"), the optical injection enslaves the laser. The laser does not emit by itself, but acts as an amplifier of the injected field. The emitted field has only two angular components at the angles $-\alpha$ and α [2-nd row panels], and its phase does not show some extended lateral oscillations around a fixed value any more [3-rd row panels].

When comparing three types of the optical injection (three columns of Fig. 6), we can recognize that only the case of both focused injected beams (column c) has no clear transition between the

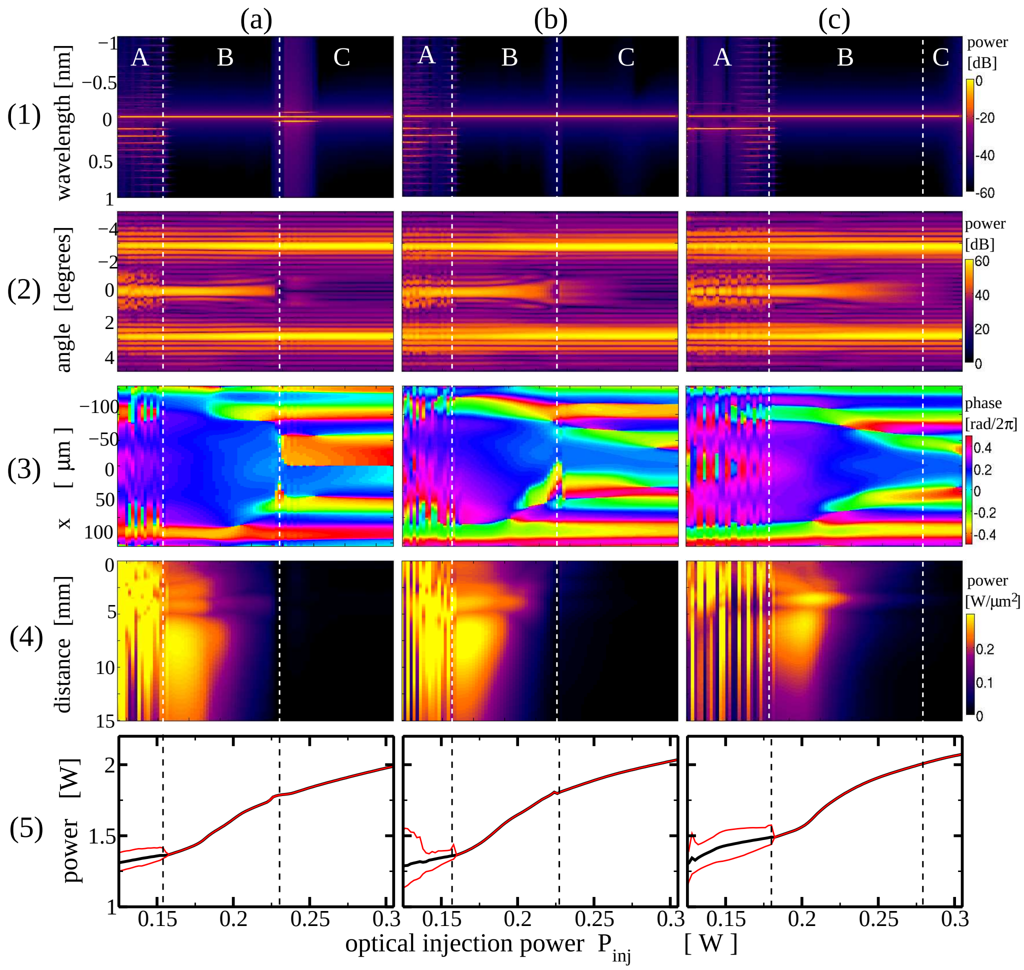

Figure 6: Dynamics of the optically injected laser ($\omega_{in} = 0$) in dependence on the increased injection power P_{inj}. Columns: same as in Fig. 5. Rows: mappings of optical spectra of the emitted field (1), its far fields (2), phases of this field after a small-scale-averaging (3), peak intensities of the small-scale-averaged field at different distances form the facet (4), and mean (black), minimal and maximal (red) power of the emitted field (5). The vertical dashed lines separate three regions with typical dynamical regimes. A: an unstable multi-mode regime. B: a stable "rocking" regime. C: a stable regime with full dominance of the optical injection.

rocking and the dominating injection regimes. It seems, that in this case we have a slightly better (longitudinal) localization of the emitted small-scale-averaged field intensity [compare panel (c4) with panels (a4) and (b4)]. We note also that the spatial rocking in this case is realized for higher P_{inj}, what is the reason of larger small-scale-averaged field intensities at $P_{inj} = 0.2W$ as it was shown in Fig. 5.

6 Conclusions

Summarizing, we show numerically that the spatial rocking in broad area semiconductor lasers can be realized by the injection of the optical field formed by two, coherently interfering at some angle, beams. We have demonstrated that rocking survives if one or both of these injected beams are focused. We have also shown, that focusing of the input beams yields the focusing of the corresponding off-axis branch of the emitted field, while the focusing of the small-scale-averaged emitted field is, in general, similar for both focused and non-focused injections.

Acknowledgments

The work of M. Radziunas was supported by DFG Research Center MATHEON "Mathematics for key technologies: Modelling, simulation, and optimization of real-world processes".The work of K. Staliunas was financially supported by Spanish Ministerio de Ciencia e Innovación and European Union FEDER through project FIS2008-06024-C03-02.

References

[1] de Valcárcel, G. J. and Staliunas, K., "Excitation of phase patterns and spatial solitons via two-frequency forcing of a 1:1 resonance," *Phys. Rev. E* **67**, 026604 (2003).

[2] Staliunas, K., Buldu, J., de Valcarcel, G., and Garcia-Ojalvo, J., "Noise-induced phase bistability via stochastic rocking," *Phys. Rev. Letters* **102**, 010601 (2009).

[3] Esteban-Martin, A., Martinez-Quesada, M., Taranenko, V., Roldán, E., and de Valcárcel, G., "Bistable phase locking of a nonlinear optical cavity via rocking: transmuting vortices into phase patterns," *Phys. Rev. Letters* **97**, 093903 (2006).

[4] Cross, M. and Hohenberg, P., "Pattern formation outside of equilibrium," *Rev. Mod. Phys.* **65**, 851–1112 (1993).

[5] Walgraef, D., [*Spatio-temporal pattern formation*], Springer, New York (1997).

[6] Staliunas, K. and Sánchez-Morcillo, V., [*Transverse patterns in nonlinear optical resonators*], Springer, Berlin (2003).

[7] Coullet, P., Lega, J., Houchmanzadeh, B., and Lajzerowicz, J., "Breaking chirality in nonequilibrium systems," *Phys. Rev. Letters* **65**, 1352–1355 (1990).

[8] Coullet, P. and Emilsson, K., "Strong resonances of spatially distributed oscillators: a laboratory to study patterns and defects," *Physica D* **61**, 119âĂŞ–131 (2002).

[9] de Valcárcel, G. and Staliunas, K., "Pattern formation through phase bistability in oscillatory systems with space-modulated forcing," *Phys. Rev. Letters* **105**, 054101 (2010).

[10] Staliunas, K., de Valcárcel, G., and Roldán, E., "Bistable phase locking in a laser with injected signal," *Phys. Rev. A* **80**, 025801 (2009).

[11] Kolpakov, S., Silva, F., de Valcárcel, G., Roldán, E., and Staliunas, K., "Experimental demonstration of bistable phase locking in a photorefractive oscillator," *Phys. Rev. A* **85**, 025805 (2012).

[12] Radziunas, M. and Staliunas, K., "Spatial rocking in broad area semiconductor lasers," *Europhysics Letters* **95**, 14002 (2011).

[13] Balsamo, S., Sartori, F., and Montrosset, I., "Dynamic beam propagation method for flared semiconductor power amplifiers," *IEEE J. Sel. Topics Quantum Electron.* **2**, 378–384 (1996).

[14] Egan, A., Ning, C., Moloney, J., Indik, R., Wright, M., Bossert, D., and McInerney, J., "Dynamic instabilities in master oscillator power amplifier semiconductor lasers," *IEEE J. Quantum Electron.* **34**, 166–170 (1998).

[15] Spreemann, M., Lichtner, M., Radziunas, M., Bandelow, U., and Wenzel, H., "Measurement and simulation of distributed-feedback tapered master-oscillator power amplifiers," *IEEE J. Quantum Electron.* **45**, 609–616 (2009).

[16] Jechow, A., Lichtner, M., Menzel, R., Radziunas, M., Skoczowsky, D., and Vladimirov, A., "Stripe-array diode-laser in an off-axis external cavity: theory and experiment," *Optics Express* **17**, 19599–19604 (2009).